Publication P2

Kristjan Tabri, Jukka Määttänen, and Janne Ranta. 2008. Model-scale experiments of symmetric ship collisions. Journal of Marine Science and Technology, volume 13, number 1, pages 71-84.

J Mar Sci Technol (2008) 13:71–84
DOI 10.1007/s00773-007-0251-z

ORIGINAL ARTICLE

Model-scale experiments of symmetric ship collisions

Kristjan Tabri · Jukka Määttänen · Janne Ranta

Received: January 19, 2007 / Accepted: June 6, 2007

Abstract This study was initiated due to the lack of experimental data on ship collisions. The feasibility of model-scale ship collision experiments was examined and a series of model-scale ship collision experiments is presented. The theoretical background for the analysis of experiments is given together with the principles of scaling. Proper scaling should assure physical similarity to the large-scale experiments conducted in the Netherlands. The Froude scaling law was followed, resulting in the improper scaling of some forces: the effects of this are discussed. The study concentrates on the dynamics of collisions. The structural response, properly scaled from the large-scale experiments, was modelled using polyurethane foam as the ship's side structure. The collision process was analysed and the results of model-scale tests, large-scale experiments, and a simple analytical model were compared, showing that there was both quantitative and qualitative agreement in the results of the experiments conducted at different scales. The analytical model yielded good quantitative assessment of the deformation energy.

Key words Model- and large-scale collision experiments · Froude scaling law · Physical similarity

1 Introduction

Due to the continuous increase in the amount of water transportation, the risk of ship collisions has been growing steadily. Collision risk can be reduced either by minimizing the probability of collisions or by reducing the consequences; however, reduction of the consequences requires a good understanding of the physical phenomena. Recent large-scale experiments of symmetric ship collisions have addressed deficiencies in understanding and discovered that the existing calculation tools fail to predict the outcomes with sufficient accuracy.[1] Inaccurate predictions indicate that the calculation models either do not include all the required phenomena or include them poorly.

Although there have been several studies of analytical models designed to simulate ship collisions, such as those of Minorsky,[2] Petersen,[3] and Pedersen and Zhang,[4] experimental data with which to study the phenomena and to validate the calculation models have nevertheless been scarce. Some of the few model-scale tests to have been carried out are reported in Motora et al.[5] In these tests, the ship model was pulled sideways with a constant force. This resulted in rather low and slowly changing acceleration with a maximum value of below 0.15 m/s^2. In real collisions, the acceleration changes rapidly over a short time. To acquire data from real collisions, several large-scale collision experiments were performed in the Netherlands. All the large-scale experiments were symmetric, which means that only a limited number of motion components were excited. Furthermore, due to ballast loading conditions in some of the large-scale experiments, severe water sloshing occurred and affected the collision dynamics.

The lack of experimental data initiated a new study with the main aim of obtaining validation data. Data from large-scale experiments are favourable as they are free from scaling effects; however, due to their expensive and complicated nature they are not feasible for

K. Tabri (✉) · J. Määttänen · J. Ranta
Helsinki University of Technology, Ship Laboratory, P.O. Box 5300, 02015 TKK, Finland
e-mail: kristjan.tabri@tkk.fi

studying a wider range of collisions. Cheaper and simpler model-scale experiments offer an alternative, but attention has to be paid to scaling in order to include properly all the relevant effects. A series of model-scale collision experiments was performed in the test basin of Helsinki University of Technology. The purpose of the tests was to provide experimental validation data for various collision scenarios. The tests aimed at obtaining precise measurements not only during contact but also for a period of time after contact.

This article concentrates on symmetric collisions and studies the feasibility of model-scale collision experiments. One aim was to provide a set of experimental validation data and to prove physical similarity between the experiments conducted at different scales. The theoretical background for analysing the experiments and the principles of scaling are presented. Scaling and designing the experimental setup were carried out using the information from large-scale experiments. Proper scaling is important to maintain physical similarity to the large-scale experiments. The Froude scaling law was followed and its advantages and disadvantages are discussed. The ship models were geometrically similar to large-scale ships with a scaling factor of 35. The force–penetration curves from the large-scale experiments were used as a reference to model the structural response. In the model-scale experiments, part of the side structure of the struck ship was replaced with polyurethane foam to produce the required structural resistance. During the tests, the motions of the models and the contact force were recorded. In this article, a single experiment is analysed thoroughly to explain the phenomena of a ship collision. The results of the model-scale tests were compared to those of large-scale experiments and to a simple analytical calculation model. Comparison with large-scale experiments was performed both in a non-dimensional form, to study the overall similarity, and also in a dimensional form, to study the quality of the experiments. Here, only the most important results will be presented and discussed; an elaborate description of the tests and the analysis is presented by Määttänen.[6]

2 Formulation of the collision problem

A collision between two ships is a dynamic process involving the motions of two bodies. The main laws covering the dynamics and the kinematics are the conservation of momentum and the equilibrium of force and energy. This article presents sufficient definitions for the analysis of symmetric collision experiments and describes the background of the process. A ship collision is called symmetric if the striking ship hits the struck ship amidships at an angle normal to it.

2.1 Collision dynamics

In symmetric ship collisions, all the motions and the forces are assumed to be limited to a single plane. Figure 1 presents the kinematics with the motions and the penetration. Here, and in subsequent sections, superscript characters A and B denote the striking and the struck ship, respectively. If a variable is described with superscript i where $i = A, B$ it means that the description is common to both ships. Coordinate systems $x^Ay^Az^A$ and $x^By^Bz^B$ have their origins fixed to the centre of gravity of the ships. These coordinate systems are used to describe the motions of the colliding ships relative to an inertial Earth-fixed coordinate system $x_0y_0z_0$. At any instant, the ship's position with respect to the inertial frame is determined by vector $\mathbf{R}_C^i$.

Angular changes γ^A and φ^B from the equilibrium position are given with respect to the inertial coordinate system. When subscript 0 is added to a motion component, its projection to the inertial coordinate system is considered, e.g., $u_0^A = \dot{\mathbf{x}}^A \cdot \mathbf{i}_0 = \mathbf{u}^A \cdot \mathbf{i}_0$. Displacement com-

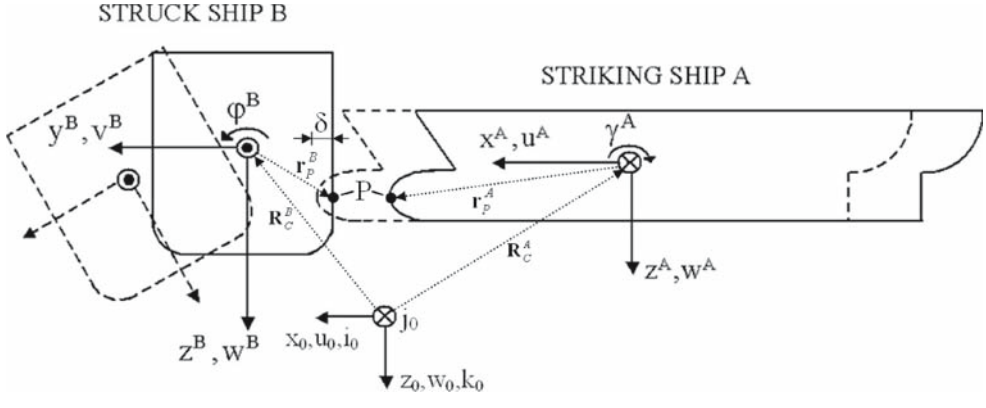

Fig. 1. Definition of collision kinematics

ponents are projected in a similar way. The translational velocity in the inertial coordinate system is thus:

$$\dot{\mathbf{R}}_C = \mathbf{u}_0 + \mathbf{w}_0 \tag{1}$$

As the motions of the ships are limited to the x_0–z_0 plane, there is only one rotational motion component for both ships and the vectors of angular velocity are simply:

$$\begin{aligned} \boldsymbol{\Omega}^A &= \gamma^A \mathbf{j}_0 \\ \boldsymbol{\Omega}^B &= -\varphi^B \mathbf{j}_0 \end{aligned} \tag{2}$$

Contact force $\mathbf{F}_C$ describes the response of the ship structures. When in contact, there is always a balance between the force and the ship motions. In Fig. 1, the letter P denotes the point where the ships first make contact. This point is described in the ship coordinate system using position vector $\mathbf{r}_P^i$. The point is fixed to the ship and does not follow the deformation of ship structures. The relative displacement between the ships, i.e., the penetration depth

$$\boldsymbol{\delta} = \mathbf{R}_C^A + \mathbf{r}_P^A - \left(\mathbf{R}_C^B + \mathbf{r}_P^B\right) \tag{3}$$

forms the kinematic condition for the collision process. Given the contact force as a function of penetration, the kinematic condition forms an important link, combining inner mechanics to external dynamics.

2.2 Energy distribution in the collision process

The analysis of ship collisions is often based on energies. Also, the proposed classification procedure by Germanischer Lloyd[7] for novel crashworthy side structures compares the energy absorption capacity of a new structure to that of a conventional structure.

There are several energy absorbing mechanisms in a collision. The major part of the energy is divided between the kinetic energy E_K of the system and the energy E_D absorbed by structural deformation. The latter is a combination of energies absorbed in different deformation processes such as tearing, stretching, crushing, and friction between the structures. However, due to the emphasis of this article, these processes are not treated separately and thus are simply referred as deformation energy. The kinetic energy of the system is the sum of the kinetic energies of both ships, which are evaluated using the velocities given in Eqs. 1 and 2. Hereinafter, when discussing the kinetic energy of a ship, the energy involved in the motions of the ship and its added mass is considered. This kinetic energy does not include the increase of the added mass over time, which is referred to as the damping part of the radiation force. Figure 2 presents a time history of the main energy components throughout contact with a duration of τ_C.

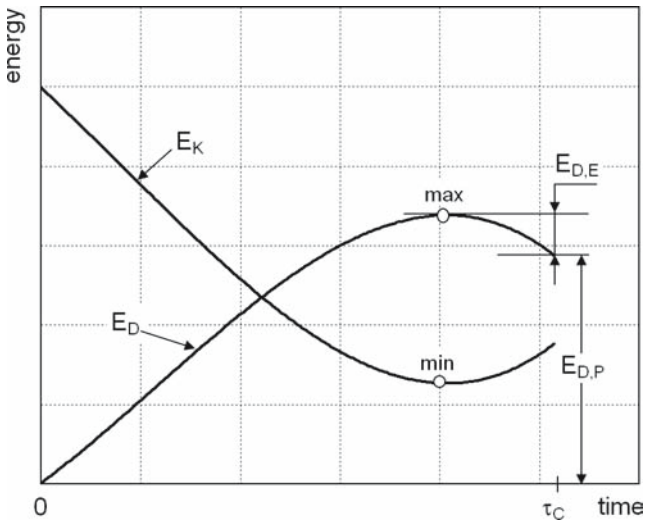

Fig. 2. Distribution of main energy components throughout the contact. E_K, kinetic energy of the system; E_D, total deformation energy; $E_{D,E}$, elastic deformation energy; $E_{D,P}$, plastic deformation energy; τ_C, duration of the contact

Let us assume that the struck ship is standing still and the striking ship is approaching with velocity $\dot{\mathbf{R}}_C^A \cong \mathbf{u}_0^A$, later referred to as the contact velocity. When the two ships collide, contact is established and the contact force obtains some value. During contact, the striking ship decelerates and loses its kinetic energy, while the struck ship gains energy through acceleration. In this energy transfer, a part of the energy is stored in deformed ship structures. This deformation energy E_D is calculated as the integral over the product of the contact force $\mathbf{F}_C$ and the penetration $\boldsymbol{\delta}$. When the velocities of both ships have equalized, the deformation energy, consisting of both elastic $E_{D,E}$ and plastic energy $E_{D,P}$, is at its maximum, while the kinetic energy of the system is at its minimum, see Fig. 2. The elastic energy stored in the structures is transferred back to kinetic energy as the elastic force starts separating the ships. The separation continues until the contact force decreases to zero. Disregarding the slow elastic recovery of the side structure, the deformation energy at that instant is equal to the plastic deformation energy.

Energy is also absorbed to overcome hydrodynamic forces such as water resistance and the damping part of the radiation force. These velocity-dependent forces do not play a major part during contact of short duration. Their importance increases when analysing the phenomena after contact. In addition to hydrodynamic forces, there are hydrostatic restoring forces. The restoring forces are significant if the displacement from the equilibrium position is large.

3 Scaling of collision experiments

3.1 Conditions for similarity

The forces involved in a collision are hydrostatic and dynamic, gravitational, inertial, and the contact force. In order to recreate a large-scale collision at model scale, the ratio of any two forces acting on the ship model must be equal to the corresponding ratio of forces in the original, i.e., dynamic similarity must be maintained. This dynamic similarity presupposes geometric similarity, as the force and pressure distribution should be geometrically similar at both scales. The importance of geometric similarity is evident as it determines the water pressure on the ship models and thus affects their position and motions. Geometric similarity is achieved by scaling the large-scale dimensions with a scaling factor λ:

$$[x_M] = \frac{[x_S]}{\lambda} \tag{4}$$

where $[x]$ represents a number of coordinates sufficient to define the shape of the hull. Subscripts M and S correspond to model and ship scale, respectively. The dimensioning of all the other parameters is thus based on λ. Dynamic similarity also presupposes kinematic similarity owing to the presence of the inertia forces. Kinematic similarity is similarity of motion, which implies both geometric similarity and similarity of time intervals. The forces present in the system must be characterized according to their origin and their relationship to some set of parameters. These reference values are the ship length l, the velocity v, the density ρ and the viscosity μ. The forces acting on the ship must be described with these parameters. Inertia forces F_I arise due to the acceleration of the ship and the surrounding water, therefore:

$$F_I \sim \rho l^2 v^2 \tag{5}$$

Gravitational forces F_G and the hydrostatic forces are due to an increase in the potential energy of the ship and can be described as:

$$F_G \sim \rho g l^3 \tag{6}$$

and the viscous shear forces F_μ can be described as:

$$F_\mu \sim \mu v l \tag{7}$$

The square root of the ratio between the inertia force and the gravity force gives the Froude number:

$$F_n = \sqrt{\frac{F_I}{F_G}} = \sqrt{\frac{\rho l^2 v^2}{\rho g l^3}} = \frac{v}{\sqrt{gl}} \tag{8}$$

whereas the ratio between the inertia force and the viscous force is the Reynolds number:

$$R_N = \frac{F_I}{F_\mu} = \frac{\rho l^2 v^2}{\mu v l} = \frac{\rho l v}{\mu} \tag{9}$$

Both of these are non-dimensional values and thus do not depend on the actual scale. Keeping the F_n value the same for both the ship model and the ship leads to the scaling law for the velocity:

$$v_M = \frac{v_S}{\sqrt{\lambda}}. \tag{10}$$

However, dynamic similarity also demands that the Reynolds numbers for the ship model and the ship are the same, in which case the model-scale velocity must be:

$$v_M = v_S \lambda. \tag{11}$$

Evidently, Eqs. 10 and 11 cannot simultaneously be satisfied, and thus model tests with the proper relationship between inertia, gravity, and viscous forces are impossible. Fortunately, viscous forces do not play a very important role in the dynamics of ship motions during such a transient event as a collision. In the collision process, inertial forces are large due to high accelerations. Velocities, especially in the case of a sideways moving struck ship, are rather low, and thus the viscous forces are small compared to the inertial forces. Considering this, the Froude scaling law (Eq. 10) was used to scale the experiments. What results is a Reynolds number that is too small and thus frictional forces are induced that are too high. As the gravity and density are constants, rough dynamic similarity is assured if the parameters are scaled accordingly:

length	$1 \sim \lambda$
area	$A \sim \lambda^2$
volume	$V \sim \lambda^3$
force	$F \sim \lambda^3$
time	$t \sim \lambda^{1/2}$
velocity	$v \sim \lambda^{1/2}$
energy	$E \sim \lambda^4$

(12)

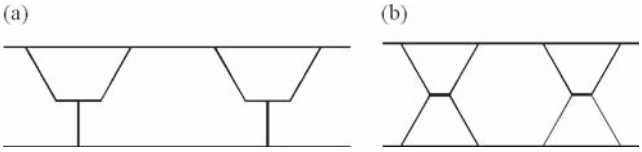

Fig. 3. Experimentally tested large-scale structures used as references for model-scale tests: Y-core structure (**a**), X-core structure (**b**)

3.2 Modelling of structural resistance

The only force not considered so far is the contact force. This force depends on the ship structures, and when scaling, the cross-sectional properties of the impact bulb and the side structure of the struck ship must be considered. Model-scale experiments concentrating on the external dynamics and the precise deformation mechanics of the structures was outside the scope of this study. However, in order to maintain dynamic similarity, the resistance has to be similar to that of large-scale ship structures. Several options to model structural resistance in model-scale ship grounding experiments were studied by Lax.[8] Considering the feasible scale for the experiments and the resistance level of different materials, polyurethane foam was chosen as a suitable material.

Several quasi-static penetration tests were conducted to find the relationship between the shape of the impact head and the contact force.[9] These tests revealed that the compression ratio for the foam was approximately 75%. For larger compression values, densification begins and the force increases rapidly. Such an increase did not occur in the large-scale experiments and thus it had to be prevented also in the model-scale tests. The dimensions of the foam block were chosen so that the predicted maximum penetration would not cause densification. The friction coefficient between the foam and the painted impact head was determined to be 0.2, which is close to the friction between two objects made of steel.

Based on the material tests, an analytical formulation was developed to estimate force–penetration curves for an impact head of arbitrary shape. Estimated curves were compared to those from the large-scale experiments with Y-core[1] and X-core[10] structures. These structures are depicted in Fig. 3 and their force–penetration curves scaled down to model scale are presented in Fig. 5. Considering the resistance level of the foam and the dimensions of the test basin, the feasible scaling factor λ was determined to be 35. Two bulbs of axisymmetric shape were manufactured with the dimensions presented in Fig. 4. The force–penetration curves obtained with these

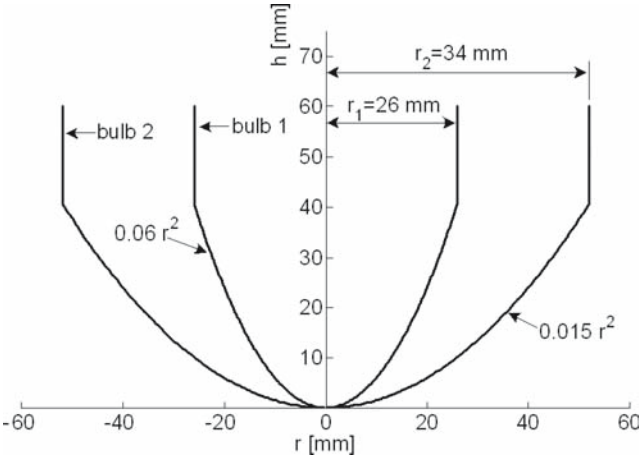

Fig. 4. Geometry of the impact bulbs used in model-scale experiments

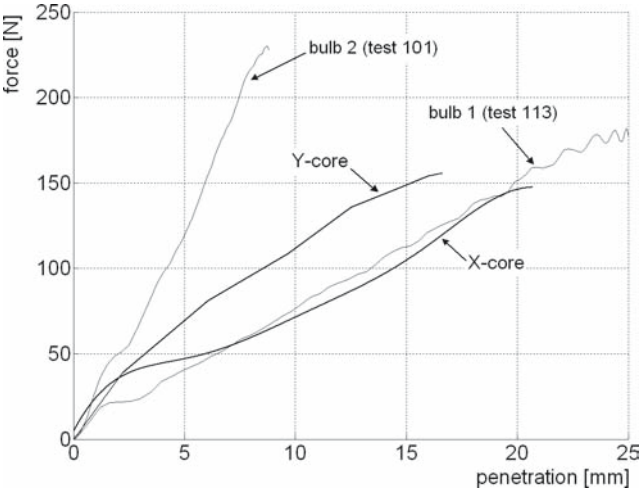

Fig. 5. Force–penetration curves in model- and large-scale experiments. Large-scale curves (X-core and Y-core) are scaled to the model scale using $\lambda = 35$

two bulbs are given in Fig. 5, in which the results of collision experiments no. 101 and 113 are presented (see Table 4). The curve of bulb 1 corresponds well to the X-core experiment, while bulb 2 produces higher resistance compared to the large-scale structures.

Obeying the Froude scaling law means that the process is recreated almost precisely over the contact duration, as then the inertia and the contact force are the dominant forces. When contact is lost, the main external forces will be the radiation force and the sway steady motion resisting force. The first behaves as an increase in the ship mass and has properties similar to inertia forces. The latter is a viscous force and, due to improper scaling, is too high. Therefore, the model-scale experiments will slightly deviate from the original behaviour

Fig. 6. Model of the struck ship

Table 1. Main linear particulars of the ship models and reference ships ($\lambda = 35$)

Ship/model	Length (m)	Breadth (m)	Depth (m)
Model A	2.29	0.234	0.12
Model B	2.29	0.271	0.12
Large-scale ship A	80	8.2	2.62
Large-scale ship B	80	9.5	2.80

λ, scaling factor; A, striking ship; B, struck ship

as time increases. This deviation is mostly absent for the contact force and the deformation energy, but increases with respect to the motions after the contact. Due to higher resistance, the ship models decelerate more and the velocities at the later stages of the collision are slightly lower compared to the original.

4 Model-scale experiments of ship collisions

4.1 Ship models and the test matrix

Ship models were scaled according to the line drawings of the ships participating in the Y-core experiment. The main particulars of the ships and the corresponding models are given in Table 1. The depth of the models was increased in order to use a larger ship mass for the different collision scenarios.

The parallel middle body of the models was made of plywood and had several transverse bulkheads to obtain sufficient stiffness. Bow and aft parts had a more complicated shape and were made of wood. Part of the port side of the struck ship model was made of polyurethane foam, as shown in Fig. 6 and Fig. 8. The foam block extended from the bow to 15 cm past amidships, amidships being the aimed contact point. The foam blocks were glued to a plywood plate that was screwed to the model with brackets. The bracket connections were of high stiffness to minimize motions between the foam block and the model.

The striking ship model was equipped with the impact bulb connected to the bow through a force sensor and an aluminium frame, see Fig. 7. The bulb and its connection to the striking ship model was essentially rigid and subject to insignificant deformations,

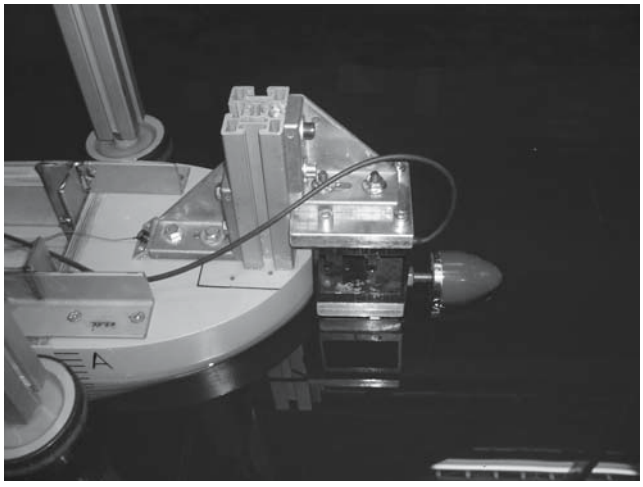

Fig. 7. The force sensor and the bulb

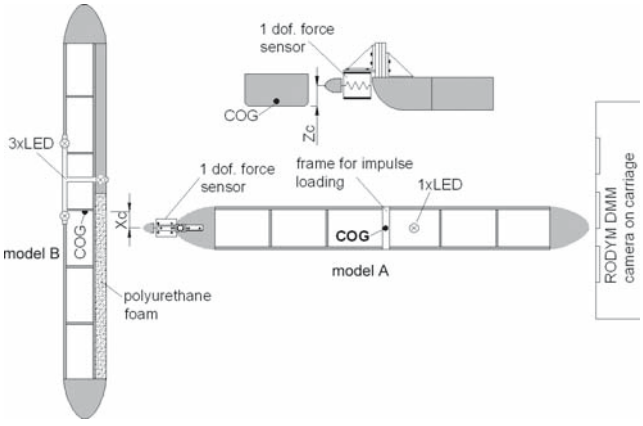

Fig. 8. General arrangement of the model tests. *dof*, degree of freedom; *LED*, light-emitting diode; *COG*, centre of gravity

which were thus disregarded. The vertical position of the bulb was adjustable to control the height of the contact point.

During collision tests, three different loading conditions were used for both ships. Table 2 presents drafts, masses, the vertical height of the centre of gravity (*KG*), and the radii of inertia k_{ii} for different loading conditions. The longitudinal centre of gravity of the struck ship was always located amidships. The table also presents the values of non-dimensional added mass coefficients μ, calculated as:

$$\mu_i = \lim_{\omega \to \infty} \frac{a(\omega)}{\rho \nabla}$$

for translational motions such as sway and heave and:

$$\mu_{ii} = \lim_{\omega \to \infty} \frac{a(\omega)}{\rho \nabla k_{ii}^2}$$

Table 2. Physical parameters of the ship models

Model	Draft (cm)	Mass (kg)	KG (cm)	k_{XX} (cm)	k_{YY} (cm)	μ_{sway} (%)	μ_{heave} (%)	μ_{roll} (%)	μ_{pitch} (%)
Striking	4	20.5	7.4	19	77	17	300	838	182
Striking	6	28.5	6.4	15	72	23	210	878	147
Striking	8	40.5	5.1	9	70	28	170	439	125
Struck	4	20.5	7.4	19	93	16	376	495	155
Struck	6	30.5	7.3	17	83	21	238	708	128
Struck	8	44.5	5.1	9	70	27	190	278	144

KG, vertical height of the centre of gravity; k_{XX}, radii of inertia with respect to longitudinal axis; k_{YY}, radii of inertia with respect to transversal axis; μ_{sway}, added mass coefficient for sway motion; μ_{heave}, added mass coefficient for heave motion; μ_{roll}, added mass coefficient for roll motion; μ_{pitch}, added mass coefficient for pitch motion

Table 3. Test matrix

Test no.	m^A (kg)	m^B (kg)	u_0^A (m/s)	Bulb	Z_C (cm)	X_C (cm)	KG^B (cm)	$Z_C - KG^B$ (cm)
101	28.5	30.5	0.39	2	7.1	11.0	7.3	–0.2
102	28.5	30.5	0.86	2	6.8	–1.5	7.3	–0.5
103	28.5	30.5	0.91	1	6.8	0.3	7.3	–0.5
104	28.5	30.5	0.45	1	7.2	6.4	7.3	–0.1
105	28.5	30.5	0.66	1	7.0	2.3	7.3	–0.3
106	20.5	30.5	0.90	1	6.1	3.3	7.3	–1.2
107	40.5	30.5	0.83	1	6.5	2.0	7.3	–0.8
108	40.5	20.5	0.83	1	4.8	1.0	7.4	–2.6
109	40.5	20.5	0.45	1	4.7	6.0	7.4	–2.7
110	28.5	20.5	0.92	1	4.8	5.0	7.4	–2.6
111	28.5	44.5	0.93	1	9.5	2.0	5.1	4.4
112	20.5	44.5	1.01	1	8.5	2.5	5.1	3.4
113	20.5	44.5	0.58	1	8.7	4.8	5.1	3.6

m^A, mass of the striking ship; m^B, mass of the struck ship; u_0^A, contact velocity; Z_C, vertical coordinate of the actual contact point; X_C, longitudinal coordinate of the actual contact point; KG^B, vertical height of the centre of gravity of the struck ship; $Z_C - KG^B$, vertical distance between the centre of gravity and the contact point

for rotational motions such as roll and pitch. Frequency-dependent added mass coefficients [$a(\omega)$] were evaluated using strip theory.[11] The surge added mass for both ship models was taken as 5% of the total mass.

The test matrix is presented in Table 3, which gives the main parameters defining the collision scenario: the masses of the ship models; the contact velocity u_0^A; the bulb type; and the coordinates X_C, Z_C of the actual contact point, as depicted in Fig. 8. The table also gives the vertical distance between the centre of gravity and the contact point $Z_C - KG$, which is an important parameter deciding the initial rolling direction of the struck model.

4.2 General arrangement of the test setup and the measuring devices

The general arrangement of the test setup is presented in Fig. 8. The striking ship model was launched towards the struck model, which was kept motionless with line reels. These reels were released just before contact. The launching of the striking ship was performed using impulse loading from a pneumatic cylinder. Loading was transferred to the striking ship model in a location close to its centre of gravity to avoid any initial pitch motion. The contact velocity was varied by adjusting the pressure in the cylinder.

Two separate measuring systems were used, one to measure ship motions and the other to record the contact force. Motions were recorded with the Rodym DMM non-contact measurement system (Krypton N.V., Leuven). This consists of a camera and infrared light emitting diodes (LEDs). The diodes blink with a certain frequency and the camera records their position. According to the position and the centre of gravity of the model, the exact location and the orientation in inertial frame $x_0y_0z_0$ is calculated. Three diodes were installed on the struck ship model and one diode was installed on the striking ship model. Three diodes allow evaluation of all six motion components, whereas one diode gives the translational components without any correction for angular motions. The sampling rate of the system was 125 Hz. In the large-scale experiments, the duration of

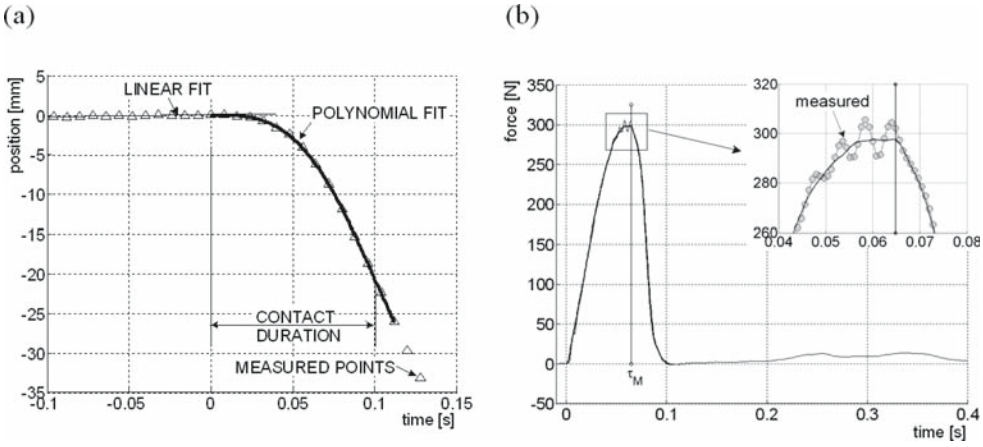

Fig. 9. Curves fitted through the measured points for the sway position of the struck ship model (test 103) (**a**) and the contact force (test 103) (**b**)

the contact was about 500 ms, which corresponds to 85 ms in the model scale. Thus, about 10 measurement points were obtained in a model-scale collision during contact.

The contact force was measured in the longitudinal direction; vertical and transverse components are assumed to be small in a symmetric collision. To minimize these force components, the tests were carried out so that the aimed contact point was not only amidships, but also vertically close to the centre of gravity of the struck ship. The force sensor, displayed in Fig. 7, consisted of an aluminium frame and a displacement sensor. The force was evaluated based on the deformation of the frame. These deformations were still negligibly small in the presumed force range. The sampling rate was 1250 Hz. After the experiment, the permanent deformation of the foam was measured with a sliding gauge to accommodate the slow elastic recovery of the foam.

4.3 Post-processing of the measurement data

The two systems were not synchronized because of a time lag resulting from the post-processing of the data in the Rodym system. According to the supplier, the duration of the time lag differs from test to test. Thus, automatic correction for the time lag was not possible and the synchronization was carried out manually. Two signals were synchronised looking at the changes in the measured signals due to contact.

Before contact, the model either is stationary or moves with a constant velocity. This is described by the straight line in Fig. 9a, which shows the sway motion of the struck ship model. The inclination of this line is the initial velocity of the model. In the figure, the line is almost horizontal, indicating that the initial velocity of the struck model was zero. When contact occurs, the behaviour changes and the straight line was replaced with a polynomial line. The point at which the polynomial met the straight line, or was closest to it, was considered to be the approximate beginning of contact. Because the frequency of the position measuring was 125 Hz, the actual beginning of contact could lie between two measurement points. The combination of linear and polynomial fit allowed the starting point to be placed between two actual measurement points. Fitted polynomials described the displacements of the models with respect to their position at the beginning of the contact. Velocities and accelerations were obtained by taking the analytical derivative of the polynomials.

When contact was initiated, the force signal rose rapidly from its initial level. As the measuring frequency for the contact force was 1250 Hz, the starting point could be detected with good accuracy, see Fig. 9b. The figure shows raw measurement data with a thin dotted line and filtered data with a bold line. The force signal had oscillatory behaviour in the vicinity of its maximum at τ_M. A possible source of the noise was vibration in the force sensor. The noise was filtered out using nonrecursive filtering[12] with a filtering window corresponding to the frequency of the noise. The time axes for the motions and the force were shifted so that time $t = 0$ s corresponded to the beginning of contact.

The quality of the synchronization was ensured by comparing the normalized force and the accelerations, see Fig. 10. The force and the accelerations were normalized and made dimensionless with respect to their maximum values. As the ships were accelerated by the contact force, all three signals should be similar and have their peak values in the same place. The water surrounding the ship models acts as a time-dependent force and thus, after reaching peak values, the accelerations do not correspond to the contact force.

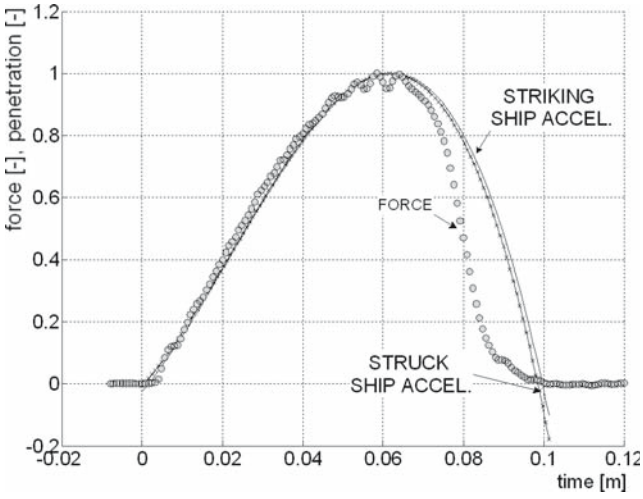

Fig. 10. Normalized accelerations in comparison to normalized contact force (test 103)

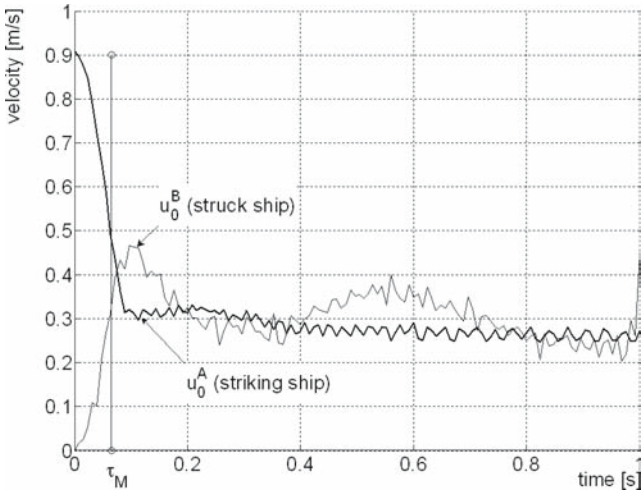

Fig. 11. Velocities of the colliding ship models (test 103). τ_M, instant of maximum contact force

5 Analysis of the results

5.1 Analysis of a collision experiment

The phenomena of a symmetric ship–ship collision is now analysed in detail by looking at a typical collision experiment. Test 103 was chosen for thorough analysis. In many subsequent figures, a vertical line is drawn at time $\tau_M = 0.065$ s, when the contact force attained its maximum value. At this time, the deformation energy, and thus also the deformations in ship structures, are supposed to be at a maximum. Figure 11 presents the main translational velocity component surge for the striking ship model and sway for the struck ship model. The force history of the test is presented in Fig. 9b. When

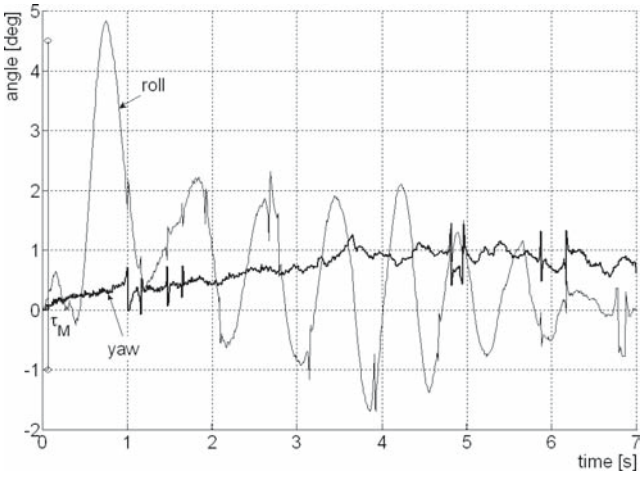

Fig. 12. Angular motions of the struck ship model (test 103)

the contact started at $t = 0$ s, the velocities of both ships started to change rapidly. After contact was lost, roughly at $t = 0.1$ s, the rapid change ceased and the velocities started to decrease slowly. The next contact occurred during the interval $t = 0.2$–0.4 s, causing some change to the velocities. Until time τ_M, the change in velocities was almost linear.

The velocity of the struck model was also influenced to some extent by rolling, even though the Rodym system considers the effects of angular motions on translational velocity. The Rodym system assumes that the rolling takes place with respect to a predefined centre of gravity. Differences arise as the centre of rolling is not exactly at the centre of gravity and, even more, the centre changes depending on whether contact is occurring or not. These two distinct phases are seen in the roll motion of the struck model presented in Fig. 12. During contact, the rolling is strongly affected by the contact force. The direction of the rolling motion depends on the distance between the centre of rolling and the contact point, given as $Z_C - KG^B$ in Table 3. The centre of rolling in a transient contact process is different from that of a free floating body. The location of the centre of roll motion is governed by the combined effect of inertia and contact and hydrodynamic forces. However, based on the experiments, a trivial conclusion can be drawn: if the contact point is clearly above the centre of gravity of the struck ship, the initial rolling angle is positive and vice versa. If the contact point is close to the centre of gravity, the rolling direction varies and the amplitude of the motion is smaller. The rolling amplitude increased when contact was lost and the contact force did not prevent free rolling. Before the maximum contact force, the angular motions were small—less than half a degree—but they increased significantly after contact.

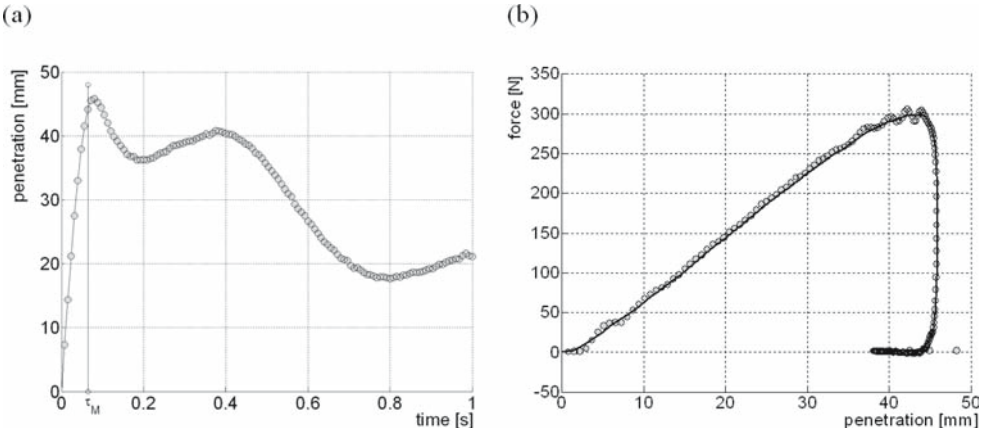

Fig. 13. Penetration depth as a function of time (**a**) and the force–penetration curve (**b**) (test 103)

The struck model usually turned slowly due to the different hydrodynamic properties fore and aft. In sideways motions, the resistance of the aft body was larger. Furthermore, as the actual location of the contact point was often located slightly away from amidships, some yaw motions were excited, as can be seen in Fig. 12.

Given the ship motions, the penetration time history was calculated using Eq. 3 and is depicted in Fig. 13a. Combining the contact force and the penetration history results in a force–penetration curve, see Fig. 13b. The penetration reached its maximum of 45.8 mm at t = 80 ms. After this, the penetration started to decrease. Contact was still maintained for some time due to immediate elastic recovery of the foam. When the contact force became zero, the penetration had a value of 42.7 mm. The final penetration value measured with the sliding gauge was 34 mm. The difference between the measured and the calculated result shows that the elastic recovery of the foam lasted longer than the duration of contact. Similar to the ship motions, the penetration increased linearly until time τ_M and then changed to more complex behaviour.

The velocities, the normalised contact force, and the normalized penetration were combined to form an overview in Fig. 14. Obviously, the penetration is at its maximum when the relative velocity between the models is zero. The figure reveals that the maximum of the penetration does not exactly coincide with that of the contact force. The same can be seen from the force–penetration curve in Fig. 13b. Looking at the filtered force signal, the difference in penetration was 1.6 mm and in time it was 13 ms.

With monotonously increasing force–penetration curves, these points should have coincided. The difference could have originated from two sources. The angular motions were not considered for the striking ship model, but any pitch or yaw increment would reduce the actual displacement of the force sensor and thus

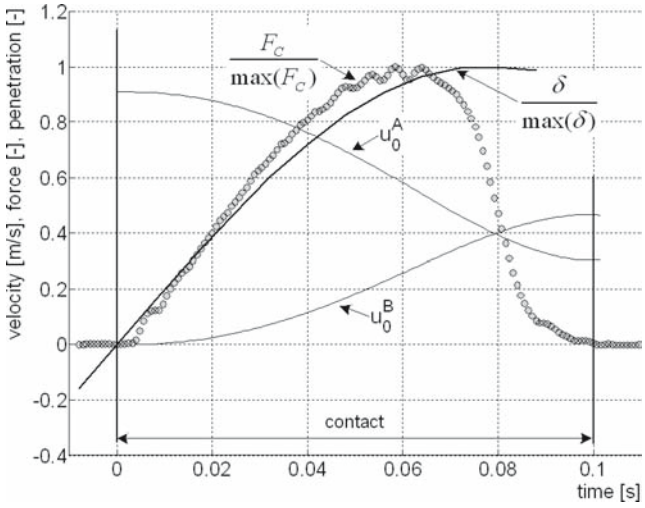

Fig. 14. Velocities of the colliding ship models, normalized contact force, and normalized penetration (test 103). F_C, contact force; δ, penetration depth

decrease the penetration value. Considering the distance between the centre of gravity and the tip of the force sensor, an error of the given magnitude would be caused by an angular motion of less than 3°. Another source could be the connection of the foam blocks to the struck ship model. Under the impact load, the whole foam block might displace slightly, and thus the actual penetration will be smaller than calculated from the displacements.

5.2 Test results and physical similarity to the large-scale experiments

The model-scale tests were intended to be physically similar to the large-scale experiments. Two different large-scale collision experiments were used to validate the similarity: collisions with X-core and Y-core side

Table 4. Large-scale collision experiments

Test	m^A (tn)	m^B (tn)	$\frac{M_A}{M_B}$ (–)	u_0^A ($t = 0$) (m/s)	E_0 (MJ)	max(δ) (m)	δ/B^B (–)	max(F_C) (MN)	E_D (MJ)	$\frac{E_D}{E_0}$ (–)	τ_c (ms)
X-core	721	2465	0.24	3.33	4.20	0.84	0.088	6.4	3.19	0.76	696
Y-core	774	1365	0.48	3.51	5.01	0.58	0.061	6.7	2.15	0.43	545
Y-core (calc.)	774	1365	0.48	3.51	5.01	0.70	0.073	7.7	3.25	0.65	490

$\frac{M_A}{M_B}$, mass ratio (including added mass); E_0, initial kinetic energy; max(δ), maximum penetration depth; δ/B^B, relative penetration depth; max(F_C), maximum contact force; E_D, total deformation energy; $\frac{E_D}{E_0}$, relative deformation energy

Table 5. Model-scale collision experiments

Test	$\frac{M_A}{M_B}$ (–)	u_0^A ($t = 0$) MS (m/s)	u_0^A ($t = 0$) LS (m/s)	E_0 MS (J)	E_0 LS (MJ)	max(δ) MS (mm)	max(δ) LS (m)	δ/B^B (%)	max(F_C) MS (N)	max(F_C) LS (MN)	E_D MS (J)	E_D LS (MJ)	$\frac{E_D}{E_0}$ (–)	τ_c MS (ms)	τ_c LS (ms)
101	0.81	0.40	2.34	2.3	3.5	9.7	0.34	4	231	9.9	1.5	2.2	0.62	60	355
102	0.81	0.88	5.18	11.5	17.2	22.7	0.80	8	540	23.1	6.2	9.3	0.54	58	341
103	0.81	0.91	5.38	12.4	18.6	45.9	1.61	17	298	12.8	7.1	10.7	0.57	101	595
104	0.81	0.46	2.75	3.2	4.8	21.3	0.74	8	147	6.3	1.7	2.5	0.52	108	637
105	0.81	0.65	3.82	6.2	9.4	33.2	1.16	12	221	9.5	3.6	5.5	0.58	98	582
106	0.58	1.00	5.91	10.7	16.1	46.1	1.61	17	296	12.7	7.7	11.6	0.72	100	592
107	1.16	0.83	4.90	14.6	21.9	40.0	1.40	15	309	13.2	7.3	10.9	0.50	105	621
108	1.78	0.82	4.82	14.1	21.2	34.8	1.22	13	260	11.2	7.2	10.8	0.51	86	506
109	1.78	0.45	2.65	4.3	6.4	24.9	0.87	9	134	5.7	1.8	2.8	0.43	102	606
110	1.26	0.92	5.45	12.7	19.1	42.2	1.48	16	278	11.9	7.0	10.6	0.55	90	532
111	0.53	0.94	5.58	13.3	20.0	61.2	2.14	23	245	10.5	9.2	13.7	0.69	157	928
112	0.38	1.01	5.95	10.9	16.4	51.6	1.80	19	301	12.9	7.8	11.7	0.72	100	592
113	0.38	0.60	3.53	3.8	5.7	25.3	0.88	9	179	7.7	2.6	3.9	0.68	100	592

MS, model scale; LS, large scale

structures.[1,10] Information about these two experiments is presented in Table 4.

The mass ratio $\frac{M_A}{M_B}$ is calculated including the surge added mass for the striking ship model and the sway added mass for the struck ship model. In the Y-core experiment, these were 0.05 and 0.24, respectively, while in the X-core experiment, the corresponding values were 0.05 and 0.29. Table 4 also presents the contact velocity u_0^A, the initial kinetic energy E_0 of the striking ship, the penetration depth δ, the maximum contact force, the combined plastic and elastic deformation energy E_D, and the duration of contact τ_c. In Table 5, the same parameters, both in model scale (MS) and equivalent large scale (LS), are presented for the model tests. In the following discussion, the model-scale tests are analysed using large-scale representation of the results.

The main parameters describing the collision dynamics are the contact velocity u_0^A and the masses of the participating ships, and these parameters have the strongest influence on the relative deformation energy. This energy is shown as a function of the mass ratio in Fig. 15, where

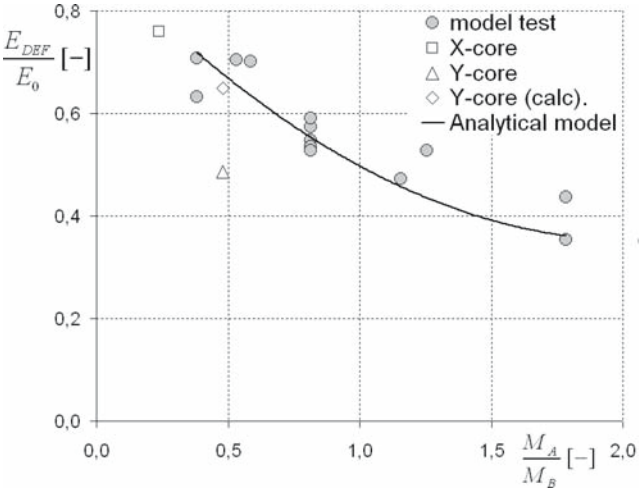

Fig. 15. Relative deformation energy (E_{DEF}/E_0) as a function of the mass ratio (M_A/M_B)

the results of the model-scale tests are presented together with the results calculated using the simple analytical formula of Minorsky[2]:

$$\frac{E_D}{E_0} = \frac{M_B}{M_A + M_B} \tag{13}$$

The figure reveals that the relative deformation energy decreases with increasing mass ratio. The X-core experiment follows the overall trend, whereas in the Y-core experiment, the relative deformation energy was lower. In the Y-core experiment, there was a large amount of water with free surface in the tanks of both ships. Water sloshing absorbs kinetic energy and thus affects the collision dynamics. Because energy was absorbed in the motions of the water, there was less energy available for structural deformation and the relative deformation energy became smaller. In Tabri et al.,[10] the Y-core experiment was recalculated without the sloshing effects and the relative deformation energy became 65%, which corresponds well to the model-scale experiments. This recalculation is referred as Y-core (calc.) in Table 4 and in Fig. 15. The simple analytical approach agrees well with the general behaviour, but as it determines the outcome based on the masses only, it does not include the effects of the velocity and structural resistance. In the model-scale experiments, these effects become apparent as experiments with the same mass ratio yield slightly different outcomes.

This non-dimensional comparison is good for quantitative assessment because the differences in input parameters vanish and the comparison is comprehensive. Even though the relative deformation energies follow the same trend, the non-dimensional representation does not yet assure the similarity. The deformation energy was calculated from the contact force and the penetration, but the penetration does not define the magnitude of the displacements. Furthermore, scaling errors might be present in both values so that they cancel each other and the error might not be obvious. Thus, it is necessary to look at dimensional values to assure the similarity. The X-core experiment was free of sloshing, but had a rather low mass ratio. Also, data from the X-core experiment is scarce, as only the force–penetration curve is presented in the literature. In the Y-core experiment, the mass ratio is similar to that of the model-scale tests and detailed data about the motions is available. Considering this, the Y-core experiment is used in the comparison.

None of the model-scale tests was an exact repetition of the Y-core experiment. Model-scale experiment number 113 was selected because of its suitable mass ratio and contact velocity. Experiments were compared,

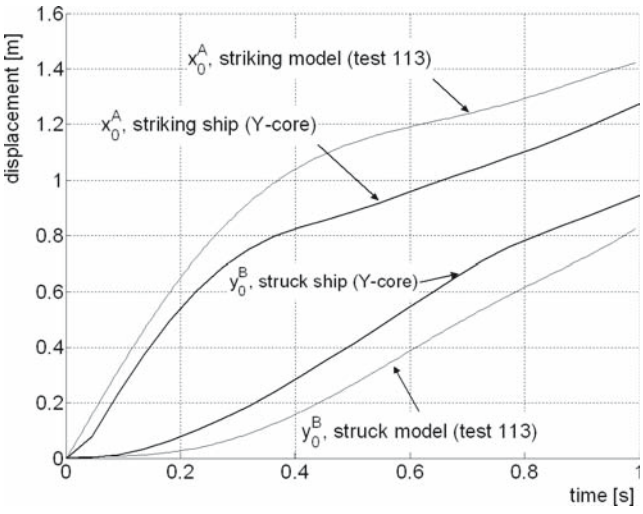

Fig. 16. Comparison of displacements in the model- and large-scale experiments

looking at the displacement and force time histories. However, the input parameters for the tests were still quite different and the histories do not match perfectly. The structural resistance in the Y-core experiment was higher than that in test 113, see Fig. 5. In addition, the model masses scaled to large-scale were higher at 879 and 1908 tons compared to 774 and 1365 tons in the large-scale experiment. The contact velocity was practically the same in both tests.

These differences are clearly reflected in the results, but the general behaviour still remains the same. The contact force depends on the inertia of the ships and on the structural resistance. The inertia of heavier ship models was larger and the changes from the initial velocity were slower. This, combined with the softer structural response, yielded smaller displacements for the struck ship model and higher displacements for the striking ship model, as seen in Fig. 16. The maximum penetration in the model-scale experiment was equivalent to 0.88 m, which was clearly higher than the 0.58 m in the large-scale experiment, as depicted in Fig. 17. The softer responses and the heavier ship models also extended the duration of contact. This can be seen from the penetration history, in which the maximum penetration occurred later, and also from the force time history in Fig. 18. The force peak was wider and the maximum force was higher. A second force peak in the large-scale experiment occurred due to sloshing. Obviously, this was not present in the model-scale experiments and the force remained at zero.

Even though a dimensional comparison was made for experiments with quite different input parameters, they still clearly demonstrate the same physical behaviour.

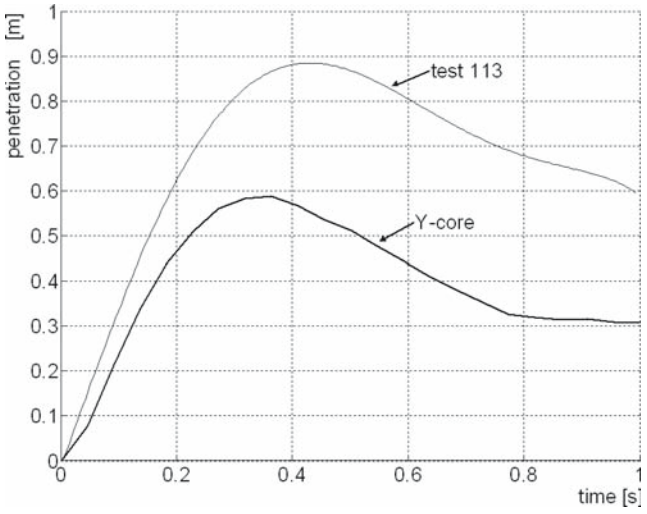

Fig. 17. Comparison of penetration in the model- and large-scale experiments

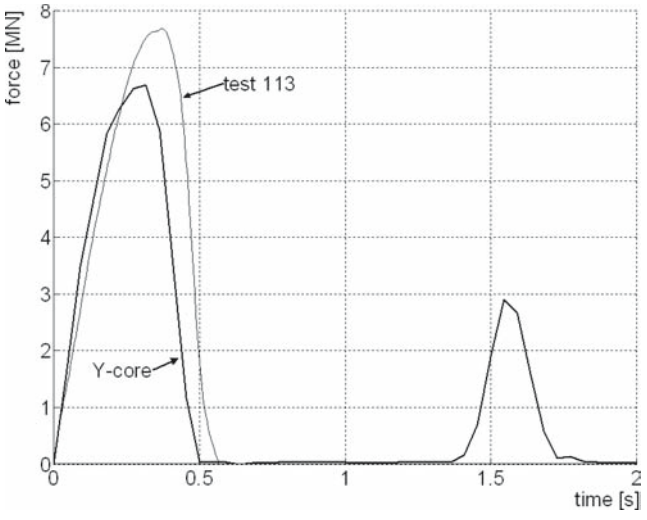

Fig. 18. Comparison of the contact force in the model- and large-scale experiments

The comparison confirmed that the model-scale experiments agreed with the large-scale experiments both quantitatively and qualitatively.

6 Conclusions

A series of symmetric model-scale ship collision experiments is presented. The feasibility of such experiments and their agreement with large-scale tests were examined. The Froude scaling law was applied with a scaling factor of 35. The ship models were geometrically similar to the large-scale ships. The structural response was modelled using polyurethane foam and an impact bulb dimensioned to result in a properly scaled force. Two measuring systems were used to record ship motions and the contact force.

Post-processing of the data resulted in some complications using the Rodym position measuring system in a transient collision process. The Rodym system modifies data before the output, causing a time lag, the length of which is hard to estimate precisely. Thus, the automatic synchronization of the two systems was impossible and so it was performed manually. Synchronization problems could be relieved by adding an acceleration sensor with a high sampling rate to the measuring system and comparing the motions obtained from it to those of the Rodym system.

A single experiment was analysed in detail to show the behaviour of ships in a collision. The analysis showed that ship motions were almost linear up to the instant when the contact force reached its maximum. After contact is lost, the behaviour becomes more complicated. The presence of linear behaviour until the maximum deformation depth allows significant simplifications in the analysis of ship collisions. Rolling and other angular motions were small during contact, because the contact force prevented large amplitude rolling of the struck ship model. After contact was lost, the rolling amplitude increased significantly. The effect of the rolling was also visible in the signals for translational motions. The Rodym system corrected the translational motions to a predefined centre of rotation, but because this position changed during the collision process, the correction did not work perfectly.

Comparison with large-scale experiments showed the physical similarity between experiments using different scales. In the non-dimensional comparison, in which the relative deformation energy was studied as a function of the mass ratio, the large-scale experiments followed the same trend as the model-scale tests. Analysis showed that the mass ratio is the most important parameter in determining the portion of total energy absorbed by ship structures in symmetric collisions. Other parameters, such as the collision velocity and structural response, have a secondary effect on the relative deformation energy. A qualitative comparison was carried out by looking at the dimensional time histories of model-scale test number 113 and of the Y-core experiment. Input parameters for those two tests were not identical, and thus the results also deviated in the expected manner. The force time history was nevertheless very similar at both scales. The comparison indicated that the model-scale experiments not only followed the same general behaviour as the large-scale experiments, but also the magnitudes of the motions and the forces agreed. Also,

the simple analytical model agreed well with the general behaviour of the experiments.

With the test setup validated using large-scale experiments and an analytical formula, the setup can be exploited to cover an even wider range of collision scenarios. Possible effects rising from arbitrary collision angles and collision locations can be studied and implemented as simulation tools.

Acknowledgments. This experimental study was carried out under the Finnish national research project TÖRMÄKE, funded by TEKES through R&D program MERIKE. This contribution and financial support is gratefully acknowledged.

References

1. Wevers LJ, Vredeveldt AW (1999) Full-scale ship collision experiments 1998. TNO- report 98-CMC-R1725, Delft, the Netherlands, p 260
2. Minorsky VU (1959) An analysis of ship collision with reference to protection of nuclear power plants. J Ship Res 3:1–4
3. Petersen MJ (1982) Dynamics of ship collisions. Ocean Eng 9:295–329
4. Pedersen PT, Zhang S (1998) On impact mechanics in ship collisions. Mar Struct 11:429–449
5. Motora S, Fujino M, Suguira M, et al (1971) Equivalent added mass of ships in collision. J Soc Nav Archit Jpn 7:138–148
6. Määttänen J (2005) Experiments on ship collisions at model scale. Master's Thesis, Helsinki University of Technology, p 145
7. Zhang L, Egge ED, Bruhns H (2004) Approval procedure concept for alternative arrangements. In: Proceedings of the 3rd international conference on collision and grounding of ships, ICCGS2004. Izu, 25–27 October, pp 87–96
8. Lax R (2001) Simulation of ship motions in grounding. Helsinki University of Technology, Report M-260, p 129
9. Ranta J, Tabri K (2007) Study on the properties of polyurethane foam for model-scale ship collision experiments. Helsinki University of Technology, Report M-297
10. Tabri K, Broekhuijsen J, Matusiak J, Varsta P (2008) Analytical modelling of ship collision based on full-scale experiments. J Mar Struct (in press)
11. Journée JMJ (1992) Strip theory algorithms. Delft University of Technology, Report MEMT 24
12. Press WH, Flannery BP, Teukolsky SA, Vetterling WT (1986) Numerical recipes: the art of scientific computing. Cambridge University Press, Cambridge, p 818